The first moment of azimuthal anisotropy in nuclear collisions from AGS to LHC energies

Subhash Singha, Prashanth Shanmuganathan and Declan Keane
Department of Physics, Kent State University, Ohio 44242, USA
(Dated: October 4, 2016)

We review topics related to the first moment of azimuthal anisotropy (v_1), commonly known as directed flow, focusing on both charged particles and identified particles from heavy-ion collisions. Beam energies from the highest available, at the CERN LHC, down to projectile kinetic energies per nucleon of a few GeV per nucleon, as studied in experiments at the Brookhaven AGS, fall within our scope. We focus on experimental measurements and on theoretical work where direct comparisons with experiment have been emphasized. The physics addressed or potentially addressed by this review topic includes the study of Quark Gluon Plasma, and more generally, investigation of the Quantum Chromodynamics phase diagram and the equation of state describing the accessible phases.

arXiv:1610.00646v1 [nucl-ex] 3 Oct 2016

I. INTRODUCTION

The purpose of relativistic nuclear collision experiments is the creation and study of nuclear matter at high energy densities. Experiments have established a new form of strongly-interacting matter, called Quark Gluon Plasma (QGP) [1–7]. Collective motion of the particles emitted from such collisions is of special interest because it is sensitive to the equation of state in the early stages of the reaction [8–10]. Directed flow was the first type of collective motion identified among the fragments from nuclear collisions [11–13], and in current analyses, is characterized by the first harmonic coefficient in the Fourier expansion of the azimuthal distribution of the emitted particles with respect to each event's reaction plane azimuth (Ψ) [14–16]:

$$v_1 = \langle \cos(\phi - \Psi) \rangle, \tag{1}$$

where ϕ is the azimuth of a charged particle, or more often, the azimuth of a particular particle species, and the angle brackets denote averaging over all such particles in all events. In some experimental analyses, v_1 is evaluated directly from Eq. (1), then a correction is applied for reaction plane resolution [15], whereas in a typical modern analysis method, the directed flow correlation is extracted using cumulants [16]. In general, v_1 is of interest when plotted as a function of rapidity, y, or sometimes pseudorapidity $\eta = -\ln(\tan\theta/2)$, where θ is the polar angle of the particle. The dependence of v_1 on collision centrality and on transverse momentum, p_T, can offer additional insights.

Until relatively recently [17, 18], the rapidity-even component $v_1^{\rm even}(y) = v_1^{\rm even}(-y)$ was always assumed to be zero or negligible in mass-symmetric collisions. In fact, fluctuations within the initial-state colliding nuclei, unrelated to the reaction plane, can generate a significant $v_1^{\rm even}$ signal [17, 18]. This fluctuation effect falls beyond the scope of the present review, which focuses on fluid-like directed flow, $v_1^{\rm odd}(y) = -v_1^{\rm odd}(-y)$, as per Eq. (1), and from here on, v_1 for mass-symmetric collisions implicitly signifies $v_1^{\rm odd}$.

During the first decade of the study of v_1 in nuclear collisions, it was more commonly called sideward flow. It refers to a sideward collective motion of the emitted particles, and is a repulsive collective deflection in the reaction plane. By convention, the positive direction of v_1 is taken to be the direction of 'bounce-off' of projectile spectators in a fixed target experiment [8, 10]. Models imply that directed flow, especially the component closest to beam rapidities, is initiated during the passage time of the two colliding nuclei; the typical time-scale for this is $2R/\gamma$ [9, 10], where R and γ are the nuclear radius and Lorentz factor, respectively. This is even earlier than the still-early time when elliptic flow, v_2, is mostly imparted. Thus v_1 can probe the very early stages of the collision [19, 20], when the deconfined state of quarks and gluons is expected to dominate the collision dynamics [9, 10]. Both hydrodynamic [21, 22] and transport model [23, 24] calculations indicate that the directed flow of charged particles, especially baryons at midrapidity, is sensitive to the equation of state and can be used to explore the QCD phase diagram.

The theoretical work leading to the prediction of collective flow in nuclear collisions evolved gradually. In the mid-1950s, Belenkij and Landau [25] were the first to consider a hydrodynamic description of nuclear collisions. During the 1970s, as the Bevatron at Lawrence Berkeley National Lab was converted for use as the first accelerator of relativistic nuclear beams, the idea of hydrodynamic shock compression of nuclear matter emerged [26–28], and these developments in turn led to increasingly realistic predictions [11, 12, 29] that paved the way for the first unambiguous measurement of directed flow at the Bevalac in the mid-1980s [13]. A frequent focus of theory papers during the subsequent years was the effort to use directed flow measurements to infer the incompressibility of the nuclear equation of state in the hadron gas phase and to infer properties of the relevant momentum-dependent potential [8, 10]. The observed directed flow at AGS energies [30–37] and below is close to a linear function of rapidity throughout the populated region, and the slope dv_1/dy can adequately quantify the strength of the signal. At SPS energies and above [38–46], a more complex structure is observed in $v_1(y)$, with the slope dv_1/dy in the midrapidity region being different from the slope in the regions closer to beam rapidities.

Various models also exhibit this kind of behavior. At these energies, both hydrodynamic and nuclear transport calculations predict a negative sign for charged particle dv_1/dy near midrapidity, where pions are the dominant particle species. This negative dv_1/dy near midrapidity has been given various names in the literature: "third flow component" [47], "anti-flow" [48], or "wiggle" [10, 22, 49]. This phenomenon has been discussed as a possible QGP signature, and a negative dv_1/dy for baryons has been argued [22] to be particularly significant. However, some aspects of anti-flow can be explained in a model with only hadronic physics [49, 50] by assuming either incomplete baryon stopping with a positive space-momentum correlation [49], or full stopping with a tilted source [51].

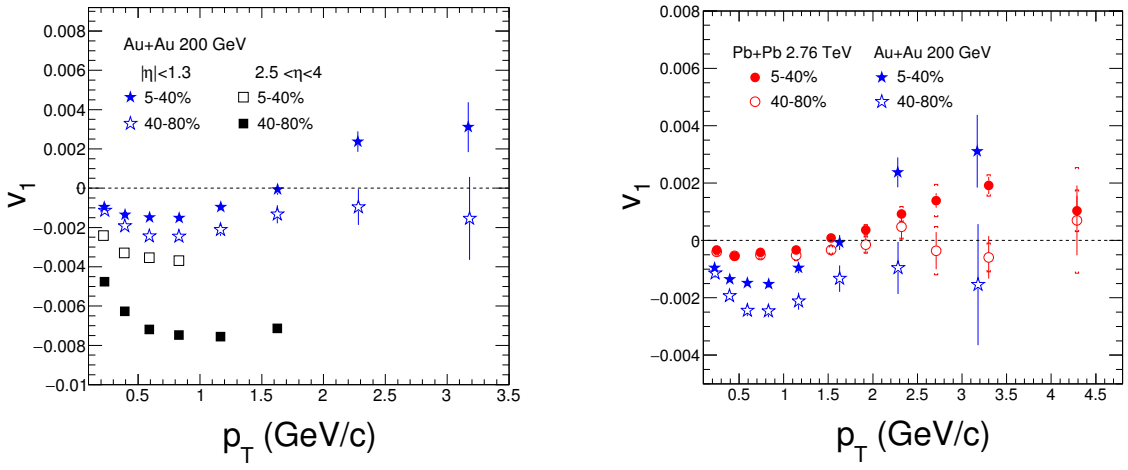

FIG. 1. (Color online) Left panel: Charged particle v_1 as a function of transverse momentum in 200 GeV Au+Au collisions at RHIC, for two centralities and two pseudorapidity windows ($|\eta| < 1.3$ and $2.5 < \eta < 1.3$) [43]. Right panel: Comparison of RHIC results with midrapidity measurements in 2.76 TeV Pb+Pb collisions at the LHC [55].

A three-fluid hydrodynamic model [22] predicts a monotonic trend in net-baryon directed flow versus beam energy in the case of a purely hadronic equation of state, whereas a prominent minimum at AGS energies, dubbed the "softest point collapse", is predicted when the equation of state incorporates a first-order phase transition between hadronic and quark-gluonic matter. Recent measurements of both proton and net-proton directed flow at RHIC [46] indeed indicate non-monotonic directed flow as a function of beam energy, with the minimum lying between 11.5 and 19.6 GeV in $\sqrt{s_{NN}}$. However, more recent hydrodynamic and nuclear transport calculations which incorporate significant theoretical improvements (see Section V) do not reproduce the notable qualitative features of the data, and therefore cast doubt on any overall conclusion about the inferred properties of the QCD phase diagram. Directed flow has also been measured at the LHC [55]. A negative slope of $v_1(\eta)$ is observed for charged particles, but its magnitude is much smaller than at RHIC, which is thought to be a consequence of the smaller tilt of the participant zone at the LHC.

In this article, we review a representative set of directed flow results spanning AGS to LHC energies. In Sections II and III, we discuss measurements of v_1 for charged particles in mass-symmetric and mass-asymmetric collisions, respectively. In Section IV, we cover measurements of v_1 for various identified particle species. Section V reviews some recent model calculations which lend themselves to direct comparisons with directed flow data. Section VI presents a summary and future outlook.

II. DIFFERENTIAL MEASUREMENTS OF CHARGED PARTICLE DIRECTED FLOW

In this section, we review measurements of v_1 for all charged particles in cases where individual species were not identified. Studies of the dependence on transverse momentum p_T, pseudorapidity η, beam energy $\sqrt{s_{NN}}$, system size, and centrality are included.

A. Dependence of v_1 on transverse momentum

The p_T-dependence of v_1 for charged particles has been studied by the STAR experiment at RHIC [42, 43]. The left panel of Fig. 1 presents directed flow results for Au+Au collisions in two centrality intervals: 5-40% and 40-80%, and in two regions of pseudorapidity: $|\eta| < 1.3$ and $2.5 < |\eta| < 1.3$. In this case, because of the odd-functional property of $v_1(\eta)$, the backward pseudorapidity region by convention has its sign of v_1 reversed before summing over the indicated gate in pseudorapidity. These measurements represent the first instance of using only spectators to determine the estimated azimuth of the reaction plane [52–54].

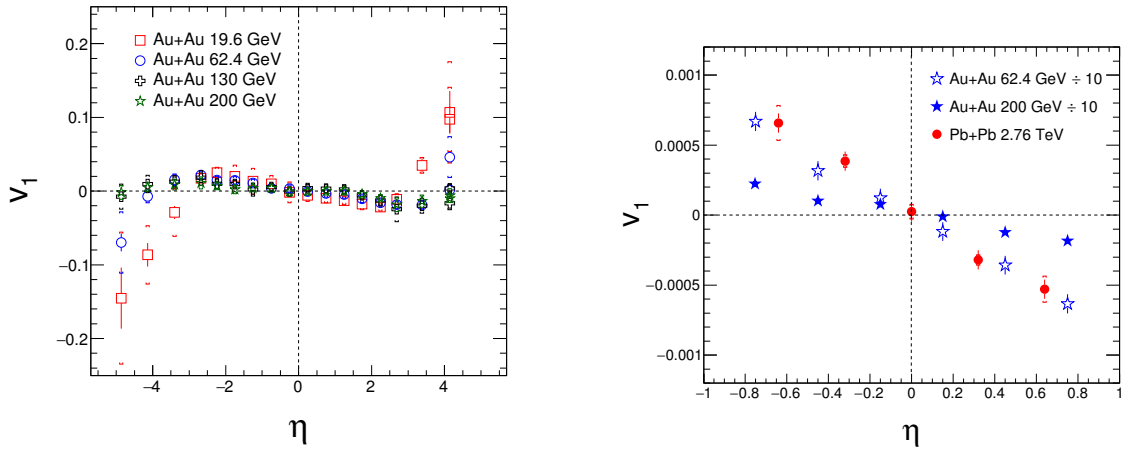

FIG. 2. (Color online) Left panel: Charged particle v_1 as a function of η for 0-40% central Au+Au collisions at $\sqrt{s_{NN}}$ = 19.6, 62.4, 130 and 200 GeV, measured by PHOBOS at RHIC [41]. Right panel: Comparison of charged particle v_1 vs. η at RHIC [43] and LHC [55] energies. Note that all the RHIC data points are divided by 10 in order to be plotted on a common scale with LHC results.

The measured v_1 in the mid-pseudorapidity interval $|\eta| < 1.3$ crosses zero in the p_T region of 1 to 2 GeV/c. Extrapolations raise the possibility that a qualitatively similar zero crossing by forward-pseudorapidity v_1 occurs at higher p_T, but that region does not fall within the acceptance of the STAR detector.

The charged particle $v_1(p_T)$ measurements by ALICE [55] in Pb+Pb collisions at 2.76 TeV are compared in the right panel of Fig. 1 with the corresponding data from 200 GeV Au+Au collisions at RHIC. The measurements at both LHC and RHIC shows a similar trend, including a sign change around $p_T \sim 1.5$ GeV/c in central collisions and negative values at all p_T for peripheral collisions.

There is an interest in the observation of zero crossing behavior in $v_1(p_T)$ as it can be used to constrain hydrodynamic model calculations [56]. It has been pointed out that this sign change is an artifact of combining all species of charged particles together, and can be explained [43] by the different sign of v_1 for pions and baryons, in conjunction with the enhanced production of baryons at higher p_T [57]. This complication is one of the reasons why directed flow of identified particles, as reviewed in later sections, can be easier to interpret and offers additional insights.

B. Dependence of v_1 on pseudorapidity

The left panel in Fig. 2 shows charged particle $v_1(\eta)$ in Au+Au collisions at 19.6, 62.4, 130 and 200 GeV measured in the PHOBOS detector [41]. It is evident that charged particle v_1 within 3 to 4 units of η on either side of $\eta = 0$ has a sign opposite to that of the spectators on that side of $\eta = 0$ (the anti-flow phenomenon).

The right panel of Fig. 2 shows the η dependence of v_1 for charged particles in 2.76 TeV Pb+Pb collisions, as measured by the ALICE collaboration [55] at the LHC. The ALICE results are compared in this panel with RHIC measurements from STAR [40, 43]. The v_1 slope at the LHC and at the top RHIC energies has the same negative sign, but the slope magnitude at the LHC is a factor ~ 3 smaller than at top RHIC energy. This pattern is consistent with the participant zone at the LHC having a smaller tilt, as predicted [51], and does not support a proposed picture at LHC energies in which a strong rotation is imparted to the central fireball [58, 59].

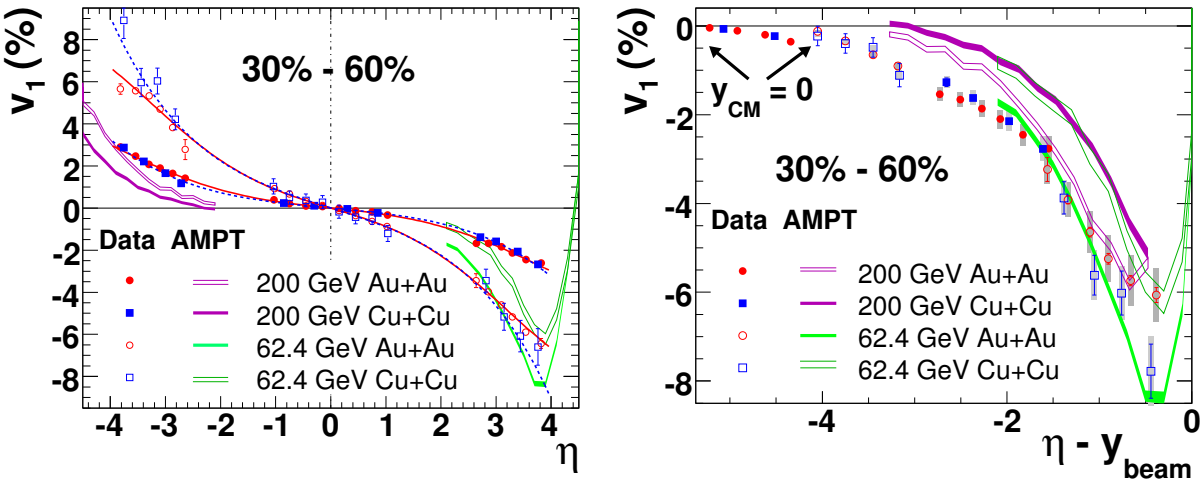

FIG. 3. (Color online) Left panel: Charged particle v_1 as a function of η for 200 and 62.4 GeV Au+Au and Cu+Cu collisions [43]. Right panel: the same as the left panel, but with the x-axis shifted by $y_{\rm beam}$.

C. System size and beam energy dependence of v_1

The beam energy and system size dependence of v_1 have been studied at RHIC using data from two colliding species at two beam energies. The left panel of Fig. 3 shows charged particle v_1 for mid-centrality (30-60%) Au+Au and Cu+Cu collisions at $\sqrt{s_{NN}} = 62.4$ and 200 GeV, measured by STAR [43]. A trend of decreasing $v_1(\eta)$ is observed as beam energy increases for both Au+Au and Cu+Cu collisions. Across the reported pseudorapidity range, $v_1(\eta)$ is independent of system size within errors at each beam energy. This is a remarkable finding, given that the Au+Au system mass is three times that of the Cu+Cu system, and given that neither the AMPT [60–62] nor the UrQMD [23, 24] models exhibit such a scaling behavior.

A different scaling behavior is presented in the right panel of Fig. 3. Here, the data in the left panel are transformed into the rest frame of the beam nucleus, i.e., zero on the x-axis corresponds to $y_{\rm beam}$ for each of the two collision energies involved. Within errors, the measurements lie on a universal curve across about three units of pseudorapidity. This behavior is known in the heavy-ion literature as limiting fragmentation, and had previously been observed in Au+Au collisions as a function of beam energy by STAR [42] and PHOBOS [41]. The term 'limiting fragmentation' was originally employed by Feynman [63] and Benecke *et al.* [64] to describe the analogous phenomenon of the measured μ^+/μ^- ratio in cosmic ray showers at sea level being almost independent of muon energy.

D. Centrality dependence of v_1

Fig. 4 shows v_1 as a function of collision centrality in 62.4 and 200 GeV Au+Au [43] from STAR and in 2.76 TeV Pb+Pb [55] from ALICE, for the mid-pseudorapidity region $|\eta| < 1.3$. Fig. 4 also shows v_1 (divided by 6 in order to fit conveniently on a common scale) as a function of collision centrality in 200 GeV Au+Au [43] from STAR at the forward pseudorapidity region $2.5 < |\eta| < 4.0$.

Directed flow magnitude at mid-pseudorapidity increases monotonically going from central to peripheral collisions at all three beam energies, and there is a strong trend for this magnitude to decrease with increasing beam energy. A similar but stronger centrality dependence is observed at forward pseudorapidity, and the magnitude also increases strongly from mid to forward pseudorapidity.

It has been pointed out by Caines [65] that many aspects of soft physics (defined as $p_T < 2$ GeV/c) in heavy-ion collisions at relativistic energies depend only on event multiplicity per unit rapidity; in other words, for a fixed value of $dN_{\rm ch}/d\eta$, there is no significant dependence on beam energy, or on centrality, or on the mass of the colliding system. This type of scaling is called "entropy-driven" soft physics. The directed flow results for two beam energies and two colliding systems reported by STAR in Ref. [43] (see Fig. 3) represented one of the first (and still few) violations of entropy-driven multiplicity scaling. In contrast, this

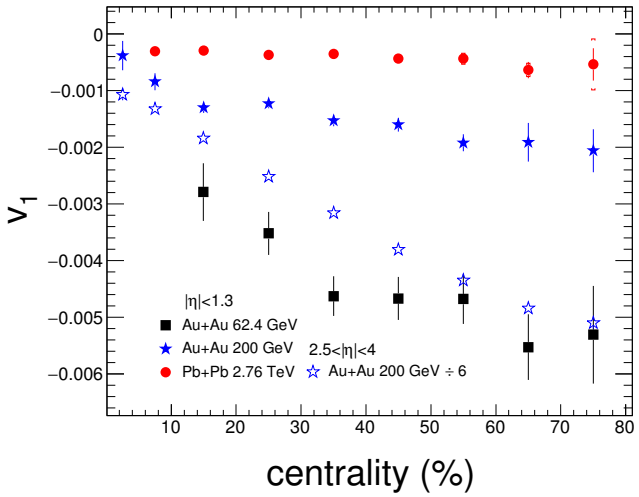

FIG. 4. (Color online) v_1 of charged particles as a function of centrality for a mid-pseudorapidity region ($|\eta| < 1.3$) and a forward pseudorapidity region ($2.5 < |\eta| < 4.0$). Two RHIC datasets, 62.4 and 200 GeV Au+Au [43] and one LHC dataset, 2.76 TeV Pb+Pb [55] are shown at mid-pseudorapidity, while only 200 GeV Au+Au [43] is shown at forward pseudorapidity. Note that the data points at forward pseudorapidity are divided by 6 in order to be plotted on a common scale with the data at mid-pseudorapidity.

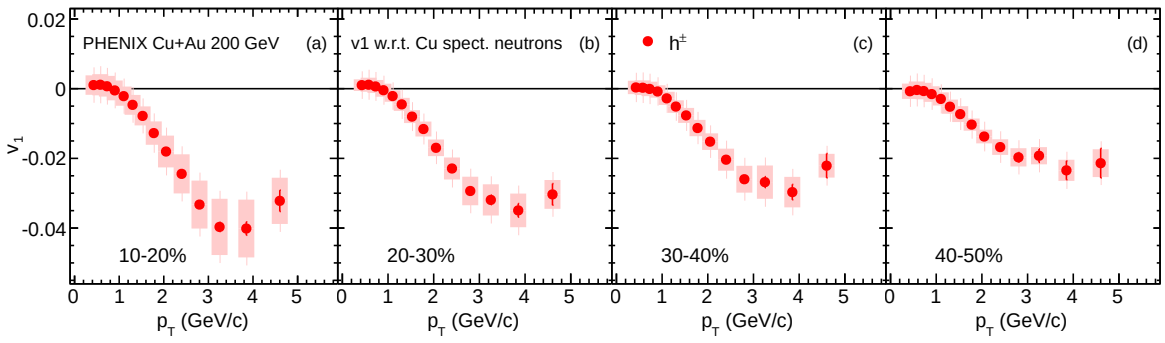

FIG. 5. (Color online) Midrapidity $v_1(p_T)$ in Cu+Au collisions at $\sqrt{s_{NN}} = 200$ GeV in four bins of centrality, as reported by the PHENIX collaboration [69].

scaling is observed to hold, with caveats, for homogeneity lengths from femtoscopy [65, 67], for elliptic flow per average participant eccentricity [65, 68], and for various strangeness yields [65]. More recent data from the LHC also reveal examples of entropy-driven multiplicity scaling [66].

III. DIRECTED FLOW OF CHARGED PARTICLES IN MASS-ASYMMETRIC COLLISIONS

In mass-asymmetric collisions like Cu+Au, the well-defined distinction that exists in mass-symmetric collisions between the odd $v_1(\eta)$ component (a hydrodynamic effect correlated with the reaction plane) and the even $v_1(\eta)$ component (an initial-state fluctuation effect unrelated to the reaction plane) no longer holds. In a recent paper from the PHENIX collaboration, they report midrapidity charged hadron $v_1(p_T)$ in Cu+Au collisions at $\sqrt{s_{NN}} = 200$ GeV for centralities of 10-20%, 20-30%, 30-40% and 40-50%, using

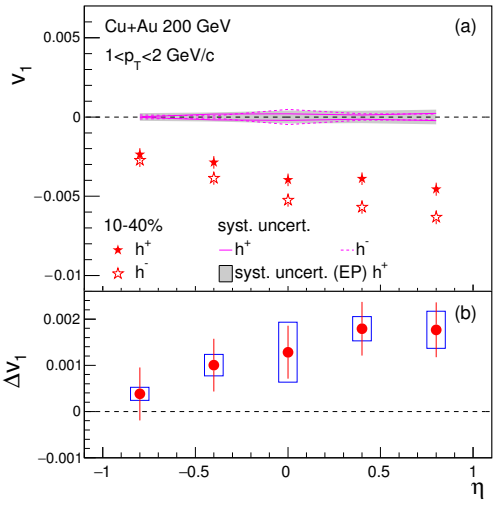

FIG. 6. (Color online) Directed flow as a function of pseudorapidity, separately evaluated for positively and negatively charged particles, at $1 < p_T < 2$ GeV/c and centrality 10-40% in 200 GeV Cu+Au collisions in the STAR detector [70].

spectator neutrons from the Au side of the collision to determine the event plane; see Fig. 5 [69]. However, they preserve the standard convention for the sign of v_1 by defining the direction of bounce-off by remnants of the first nucleus in the A+A system (Cu) to be positive. An even more recent paper from STAR reports $v_1(p_T)$ distributions for the same system and centrality that are consistent within errors [70].

The PHENIX results in Fig. 5 [69] reveal that the higher p_T particles at midrapidity (above 1 or 1.5 GeV/c in p_T), and at all the studied centralities, have negative v_1 and so are preferentially emitted with azimuths parallel to the Au fragment bounce-off direction (and antiparallel to the Cu fragment bounce-off direction). Whether or not the more abundant particles below 1 GeV/c are preferentially emitted with opposite azimuths, as might be expected based on momentum conservation, cannot be answered within the systematic uncertainty of the measurements [69].

In the STAR collaboration's analysis of charged particle directed flow in Cu+Au collisions at $\sqrt{s_{NN}} = 200$ GeV, a particular focus is the v_1 difference between positive and negative charges. This difference has the potential to be sensitive to the strong electric field between the two incident ions, whose electric charges differ by $79 - 29 = 50$ units; this field has a lifetime on the order of a fraction of a fm/c. Fig. 6 [70] presents $v_1(\eta)$ at medium p_T ($1 < p_T < 2$ GeV/c) and intermediate centrality (10-40%). Like the PHENIX result, this v_1 measurement was made relative to the event plane from spectator neutrons, dominated by the Au side. It is evident from Fig. 6 that both even and odd components are present, and most interestingly, there is a significant pattern showing a larger magnitude for negative particles.

The Parton-Hadron String Dynamics (PHSD) model [71, 72], when the initial electric field is explicitly modeled, predicts a v_1 difference signal that is an order of magnitude larger than observed [70]. On the other hand, parton distribution functions [73] can be used to estimate the number of quarks and antiquarks at very early times in relation to the number created in the collision; then given certain plausible assumptions, as set out in Ref. [70], it can be inferred that only a small fraction of the total quarks created in the collision are produced during the lifetime of the initial electric field. In addition to this important insight, the charged-dependent directed flow measurements in Cu+Au collisions offer new and valuable quantitative information with relevance to the Chiral Magnetic Effect [74, 75] and the Chiral Magnetic Wave [76, 77].

IV. DIFFERENTIAL MEASUREMENTS OF IDENTIFIED PARTICLE DIRECTED FLOW

The charged particle measurements reviewed in Section II are an admixture of all emitted particle species. Measurements of directed flow for identified particles offer more insights into the underlying physics that

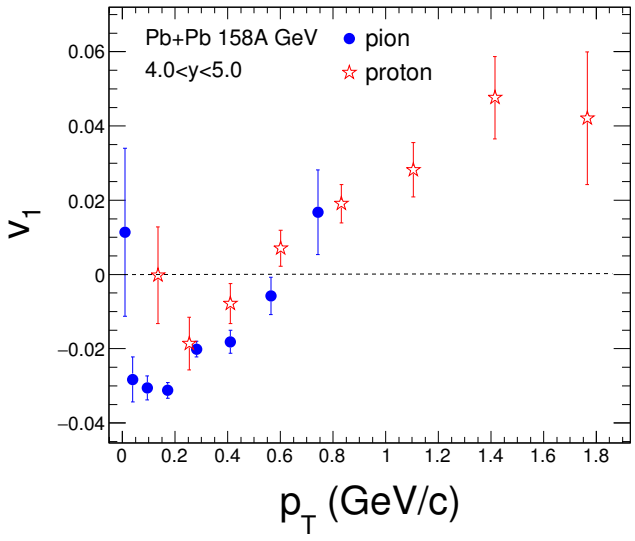

FIG. 7. (Color online) Pion and proton $v_1(p_T)$ at $4 < y_{\rm lab} < 5$ in Pb+Pb collisions at the SPS, at a projectile kinetic energy of 158A GeV [38].

controls this observable. In this section, we discuss the dependence of v_1 on p_T, y and centrality for several identified particle species.

A. Dependence of v_1 on transverse momentum

Measurements of $v_1(p_T)$ for protons, antiprotons and charged pions have been reported by the E877 collaboration at the AGS (11A GeV/c) [30–33]. For antiprotons, large negative values of v_1 are observed for $p_T > 0.1$ GeV/c but with large statistical errors. For protons and charged pions, $v_1(p_T)$ in various rapidity gates have been published, and these results are also divided into various bins of transverse energy, E_T, which is a proxy for centrality. The E877 collaboration also provides the information needed to convert from their intervals of E_T into percent centrality [31].

The NA49 collaboration [38] measured proton and pion $v_1(p_T)$ in Pb+Pb collisions at a projectile kinetic energy of 158A GeV, as shown in Fig. 7. The rapidity gate for these measurements is $4 < y_{\rm lab} < 5$, which corresponds to a forward region (midrapidity is $y_{\rm lab} = 2.92$). The NA49 collaboration describes the $v_1(p_T)$ behavior as 'peculiar', especially for pions. However, they point out that negative v_1 at low p_T has been predicted by Voloshin [78], and is explained by the interaction of radial and directed flow. Various types of non-flow effect were also mentioned as possible contributors to the observed pion behavior [38].

B. Dependence of v_1 on rapidity

Various models suggest that the structure of $v_1(y)$ near midrapidity, especially the pattern for baryons, is sensitive to the QCD equation of state and therefore this signal can be used to investigate QGP production and changes of phase [8–10, 22, 79, 80]. Fig. 8 presents proton and pion $v_1(y)$ in central, mid-central and peripheral Pb+Pb collisions at projectile kinetic energies of 40A and 158A GeV [39], as reported by the NA49 collaboration at the CERN SPS. The data points at negative rapidity are mirrored from the positive side. The $v_1(y)$ for pions is similar in magnitude and shape at both 40A and 158A GeV. The proton $v_1(y)$ measurements suggest that proton anti-flow (also called wiggle) [10, 22, 47–49], which is not observed at the AGS (see Fig. 9), might begin to happen at SPS energies. However, based on detailed studies using a variety of methods, including the approach introduced by Borghini *et al.* [81], the NA49 collaboration reports that the observed pattern of proton $v_1(y)$ at SPS energies could be influenced by non-flow effects [39].

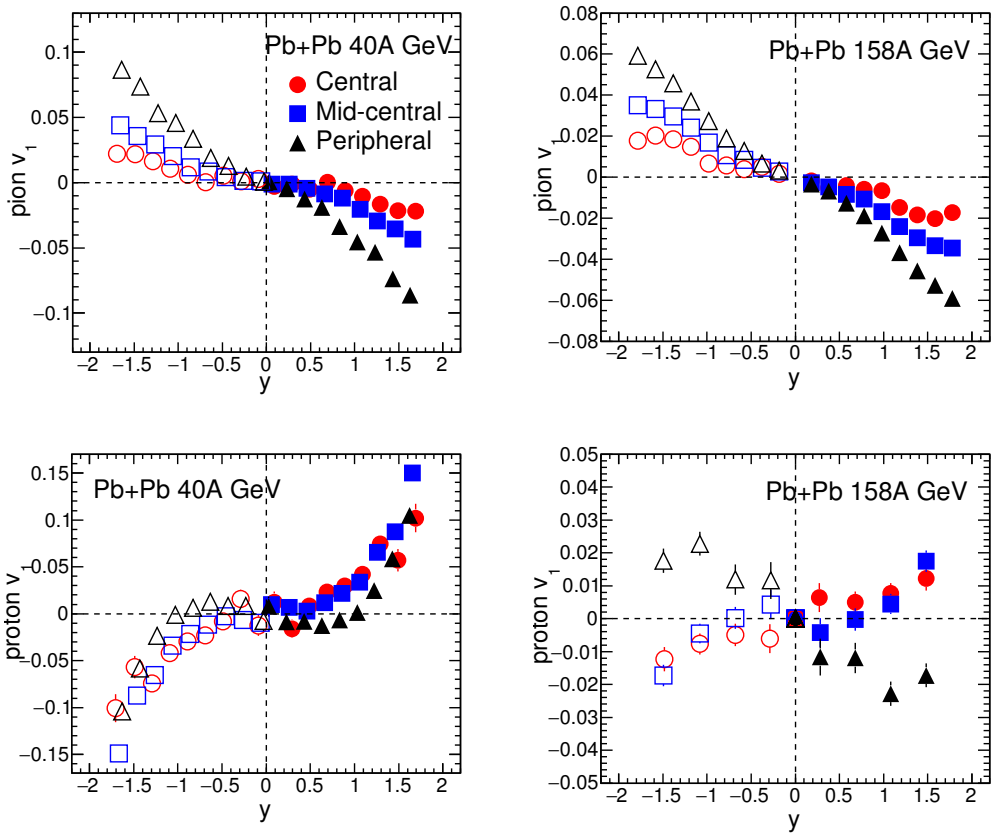

FIG. 8. (Color online) Pion and proton $v_1(y)$ for three centralities in 40A and 158A GeV Pb+Pb collisions at the SPS [39]. The open markers at negative rapidities were obtained by reflecting the solid markers at positive rapidities, where the detector acceptance was optimum.

The EOS-E895 experiment carried out a beam energy scan at the Brookhaven AGS during 1996. E895 featured the first Time Projection Chamber with pad readout, and reported directed flow in the form of v_1, as well as in the form of the older observable $\langle p_x \rangle$ [82] (in-plane transverse momentum) for several identified particle species: p, $\bar{p}$, Λ, K^0_S and $K^{\pm}$, in Au+Au collisions at projectile kinetic energies 2A, 4A, 6A and 8A GeV [34–37]. The left panel in Fig. 9 shows $v_1(y')$ for protons at the four E895 beam energies, where y' denotes normalized rapidity such that the target and projectile are always at $y' = -1$ and $+1$, respectively. The slope of v_1 remains positive for all four beam energies.

The slope of the rapidity dependence of directed flow was extracted by E895 using a cubic fit $v_1(y') = Fy' + Cy'^3$. The right panel of Fig. 9 shows the fitted proton slope dv_1/dy (not using normalized rapidity), and unlike in Ref. [34], the horizontal axis in the right panel of Fig. 9 uses the now-conventional beam energy scale $\sqrt{s_{NN}}$. Two additional points for proton dv_1/dy in Au+Au collisions are also plotted here: a measurement at the top energy of the Berkeley Bevalac (1.2A GeV) [83] using the same EOS TPC detector as in E895, and an E877 measurement at the top AGS energy of 11A GeV [31]. The plotted data show a peak near 2A GeV beam kinetic energy ($\sqrt{s_{NN}} \sim 2.7$ GeV), and thereafter, a smooth decrease with beam energy across the AGS range.

Three-fluid hydrodynamic calculations [22] predict a "softest point" in the Equation of State in the AGS energy range, but the E895 beam energy scan did not reveal any non-monotonic behavior in the energy dependence. Overall, hadronic models with a momentum-dependent mean field [84] show better agreement with data at AGS and SPS energies.

Phase-I of the beam energy scan (BES) [85, 86] at RHIC took data in 2010, 2011 and 2014, spanning the $\sqrt{s_{NN}}$ range from 200 GeV down to 7.7 GeV. Lattice QCD calculations [87–89] imply a smooth crossover from hadronic matter to QGP at beam energies near and above the top energy of RHIC, whereas phase diagram

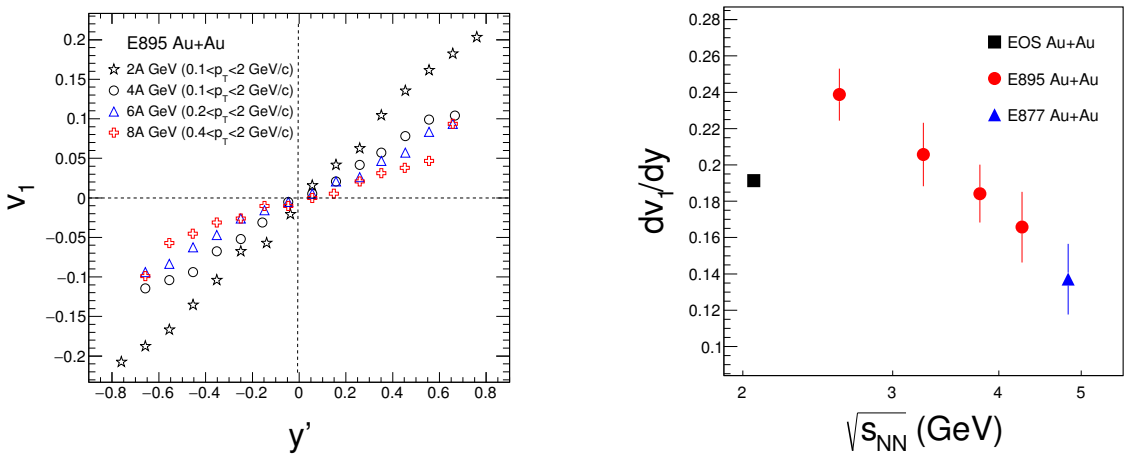

FIG. 9. (Color online) Left panel: $v_1(y')$ for protons in 2A, 4A, 6A and 8A GeV Au+Au collisions measured by E895 [34]. Right panel: Beam energy dependence of the slope dv_1/dy (here using un-normalized rapidity) for protons, re-plotted using the more ubiquitous beam energy scale $\sqrt{s_{NN}}$ [34]. A point from the same detector at the Bevalac [83] and another from E877 at the top AGS energy [31] are also plotted.

features like a first-order phase transition and a critical point may become evident in nuclear collisions as the beam energy is scanned across RHIC's BES region. The STAR experiment initially reported measurements of directed flow for protons, antiprotons and charged pions in the energy range of 7.7 to 200 GeV [46]. At the 2015 Quark Matter meeting, preliminary directed flow data at BES energies for nine particle species were presented, along with $v_1(y)$ slopes for protons, Λ and π^+ in 9 bins of centrality [90]. Fig. 10 shows $v_1(y)$ at intermediate centrality (10-40%) for p, Λ, $\bar{p}$, $\bar{\Lambda}$, $K^{\pm}$, K^0_S, and $\pi^{\pm}$ at 7.7 to 39 GeV.

The overall strength of directed flow has been characterized by the slope dv_1/dy from a linear fit over the range $-0.8 < y < 0.8$ [90], and the beam energy dependence of these slopes for the same nine particle species (p, Λ, $\bar{p}$, $\bar{\Lambda}$, $K^{\pm}$, K^0_S, and $\pi^{\pm}$) in 10-40% centrality Au+Au collisions are presented in Fig. 11.

The most noteworthy feature of the data is a minimum within the $\sqrt{s_{NN}}$ range of 10 to 20 GeV in the slope $dv_1/dy|_{y\sim 0}$ for protons at intermediate centrality. The same quantity for Λ hyperons is consistent with the proton result, but the larger statistical errors for Λ do not allow an independent determination of a possible minimum in the beam energy dependence for this species. The proton and Λ directed flow slope change from positive to negative close to 11.5 GeV, and remain negative at all the remaining energies (up to and including 200 GeV in the case of protons). The remaining species have negative slope at all the studied beam energies. At 7.7 GeV, dv_1/dy for K^- is closer to zero than dv_1/dy for K^+, which supports the inference that K^+ and K^- experience nuclear potentials that are repulsive and attractive, respectively, under the conditions created at this beam energy [91].

C. Net-particle directed flow

There are two separate contributions to the energy dependence of proton directed flow in the vicinity of midrapidity: one part arises from baryon number transported from the initial state at beam rapidity towards $y \sim 0$ by the stopping process of the collision, while the other part arises from baryon-antibaryon pairs produced in the fireball near midrapidity. Clearly, these two contributions have very different dependence on beam energy, and disentangling them has a good potential to generate new insights. Towards this end, the STAR collaboration has defined [46] net-proton directed flow according to

$$[v_1(y)]_p = r(y)[v_1(y)]_{\bar{p}} + [1 - r(y)]\,[v_1(y)]_{\text{net-}p}$$

where $r(y)$ is the observed rapidity dependence of the antiproton to proton ratio. Net-kaon $v_1(y)$ is defined analogously, with K^+ and K^- substituted for p and $\bar{p}$, respectively [90].

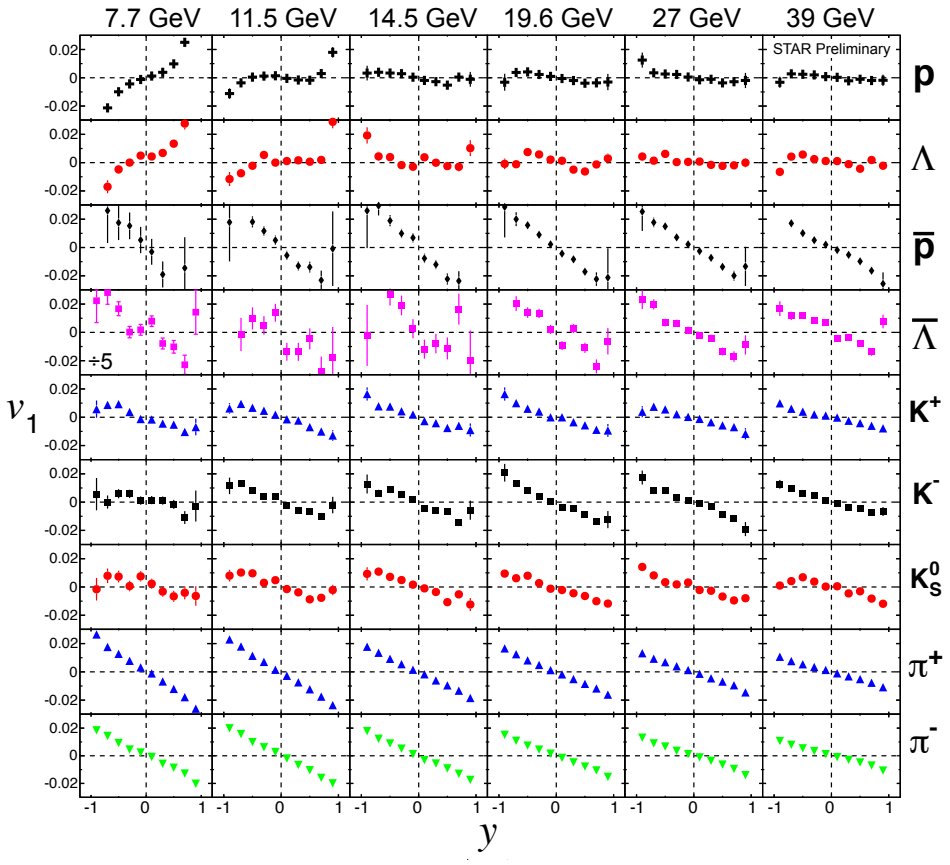

FIG. 10. (Color online) Directed flow as a function of rapidity for p, Λ, $\bar{p}$, $\bar{\Lambda}$, $K^{\pm}$, K^0_S, and $\pi^{\pm}$ in 10-40% centrality Au+Au collisions, at $\sqrt{s_{NN}}$ values of 7.7, 11.5, 14.5, 19.6, 27 and 39 GeV [46, 90]. The magnitude of v_1 for $\bar{\Lambda}$ at 7.7 GeV is divided by 5 to fit on the same vertical scale as all the other panels.

STAR's measurements of net-proton and net-kaon directed flow slope as a function of beam energy are reproduced in Fig. 12 [90]. The net-proton directed flow shows a double sign change, and a clear minimum around the same beam energy where the proton directed flow has its minimum. This coincidence is not surprising, since antibaryon production is low at and below the beam energy of the minimum, and therefore net-proton and proton observables only begin to deviate from each other at energies above the minimum.

The observed minimum in directed flow for protons and net-protons resemble the predicted "softest point collapse" of directed flow [19, 22], and these authors are open to an interpretation in terms of a first-order phase transition. Other theorists (see Section V) point out that mechanisms other than a first-order phase transition can cause a drop in pressure (a softening of the equation of state) and therefore a definitive conclusion requires more research.

The net-kaon directed flow reproduced in Fig. 12 [90] shows close agreement with the net-proton result near and above 11.5 GeV, but deviates very strongly at 7.7 GeV. This deviation is not understood. To date, all of the several model comparisons with STAR v_1 measurements at BES energies have considered only particle v_1 as opposed to net-particle v_1.

V. RECENT MODEL CALCULATIONS OF DIRECTED FLOW

Models that explicitly incorporate properties of the Quantum Chromodynamics phase diagram and its equation of state (typically hydrodynamic models) suggest that the magnitude of directed flow is an excellent indicator of the relative pressure during the early, high-density stage of the collision. Therefore, directed flow at sub-AGS beam energies can reveal information about hadron gas incompressibility, while at the

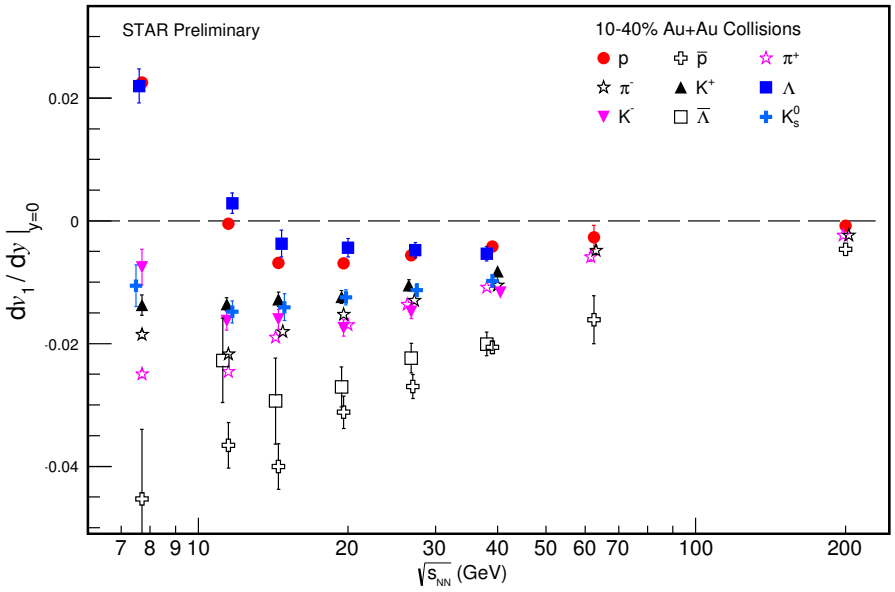

FIG. 11. (Color online) Beam energy dependence of $v_1(y)$ slope for p, Λ, $\bar{p}$, $\bar{\Lambda}$, $K^{\pm}$, K^0_S, and $\pi^{\pm}$ in 10-40% centrality Au+Au collisions [46, 90].

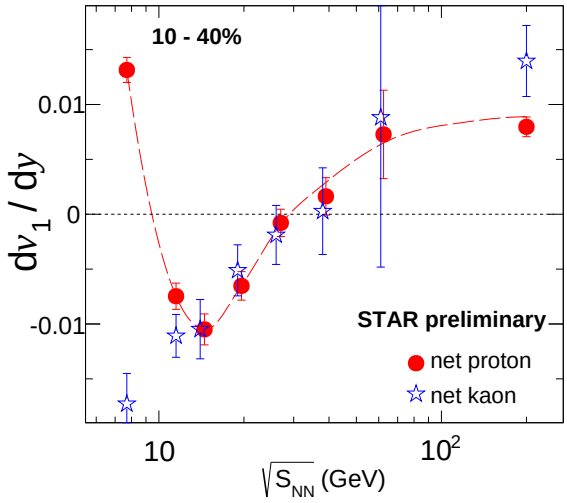

FIG. 12. (Color online) Beam energy dependence of the slope of $v_1(y)$ for net protons and net kaons in 10-40% centrality Au+Au collisions, as reported by STAR [46, 90].

higher energies that are a focus of the present review, it can flag the softening, or drop in pressure, that may accompany a transition to a different phase, notably Quark Gluon Plasma. For example, there may be a spinodal decomposition associated with a first-order phase transition [92, 93], which would cause a large softening effect. However, interpretation of flow measurements is not straightforward, and it is known that directed flow can also be sensitive to poorly-understood model inputs like momentum-dependent potentials [91] in the nuclear medium. More theoretical work is needed to elucidate the quantitative connection between softening signatures, like the beam energy dependence directed flow, and QCD phase changes.

During the period since publication of the STAR BES directed flow results in 2014, there have been several theoretical papers [19, 20, 91, 94, 95] aimed towards interpretation of these measurements. The Frankfurt hybrid model [96] used for the data comparison by Steinheimer *et al.* [94] is based on a Boltzmann transport

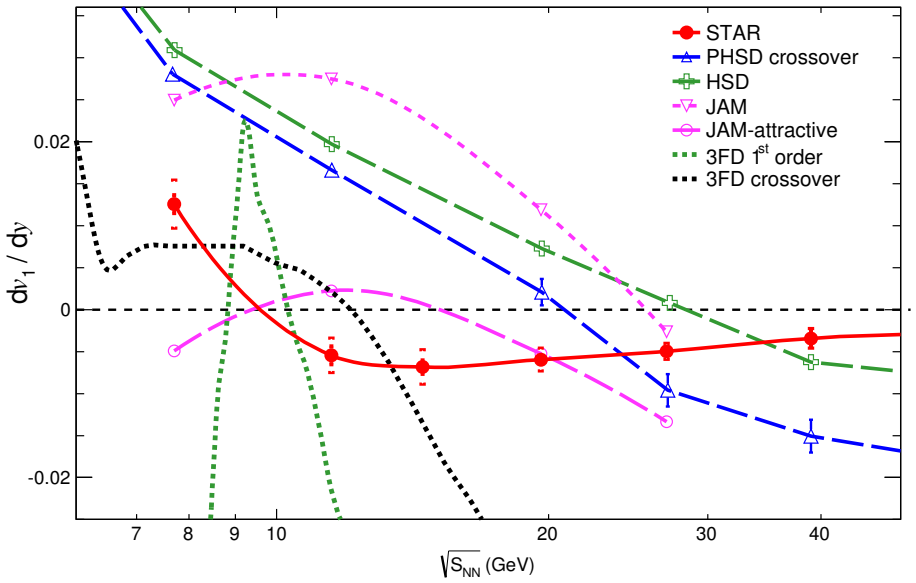

FIG. 13. (Color online) Beam energy dependence of directed flow slope for protons in 10-40% centrality Au+Au from the STAR experiment, compared with recent available model calculations [19, 20, 95]. All the experimental data are from Ref. [46] except for one energy point, $\sqrt{s_{NN}} = 14.5$ GeV [90], which should be considered a preliminary measurement. The Frankfurt hybrid model [94] as well as a pure hydro calculation with particle freeze-out at constant energy density [94] both lie above the data and are off-scale at all BES energies.

approach similar to UrQMD for the initial and late stages of the collision process, while a hydrodynamic evolution is employed for the intermediate hot and dense stage. The equation of state for the hydro stage includes crossover and first-order phase transition options. The data comparison by Konchakovski *et al.* [20] uses the Parton-Hadron String Dynamics (PHSD) model [71] of the Giessen group, a microscopic approach with a crossover equation of state having properties similar to the crossover of lattice QCD [87–89]. The PHSD code also has a mode named Hadron String Dynamics (HSD), which features purely hadronic physics throughout the collision evolution, and which yields directed flow predictions in close agreement with those [46] of the UrQMD model. The data comparison by Ivanov and Soldatov [95] uses a relativistic 3-fluid hydrodynamic model (3FD) [97] with equations of state that include a crossover option and a first-order phase transition option. The most recent comparison to the STAR BES v_1 data, by Nara *et al.* [19], uses the Jet AA Microscopic (JAM) model [98]. JAM is a purely hadronic Boltzmann transport code, but the authors of Ref. [19] introduce an option to switch from the normal stochastic binary scattering style to a modified style where the elementary 2-body scatterings are always oriented like attractive orbits [99, 100]. They argue that the switch-over from random to attractive binary orbits mimics the softening effect of a first-order phase transition.

Fig. 13 focuses on the most promising directed flow measurement from the RHIC Beam Energy Scan, namely the $dv_1/dy|_{y\sim 0}$ for protons at 10-40% centrality, and summarizes recent model comparisons [19, 20, 94, 95] with these data. These authors are largely in agreement that the data disfavor models with purely hadronic physics. However, some conclude that a crossover deconfinement transition is favored [20, 95], while others conclude that a first-order phase transition is still a possible explanation [19]. Note that the argument of Nara *et al.* [19] is that a more sophisticated implementation of a first-order phase transition would transition from the 'JAM' curve at low BES energies to the 'JAM-attractive' curve at higher BES energies.

Overall, Fig. 13 underlines the fact that no option in any of the model calculations to date reproduces, even qualitatively, the most striking feature of the data, namely, the minimum in proton directed flow in the region of $\sqrt{s_{NN}} \sim 10 - 20$ GeV. It is also noteworthy that the v_1 difference between nominally equivalent equation of state implementations in different models is very large. For example, the differences in dv_1/dy between the 1st-order phase transition in the hybrid model [94] and a similar nominal quantity for the

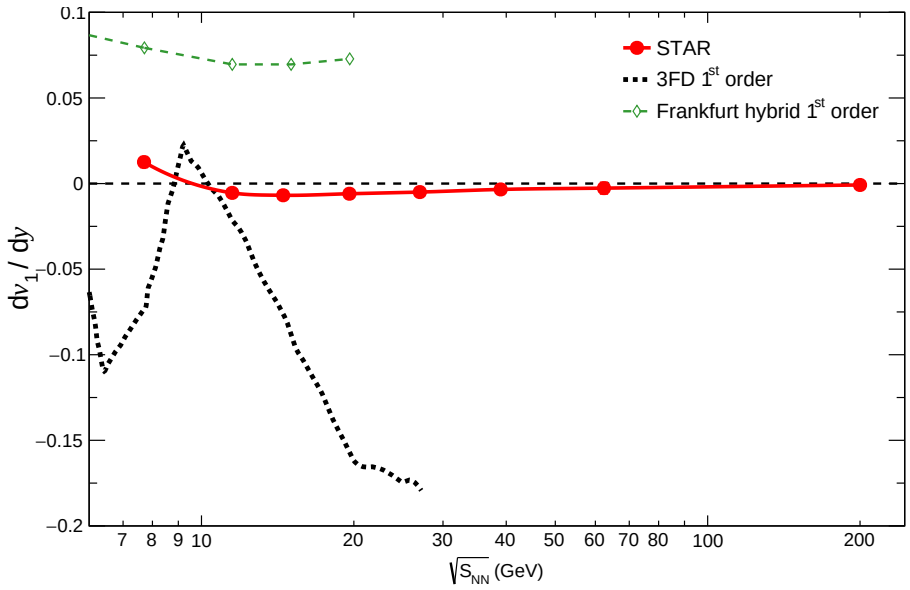

FIG. 14. (Color online) Beam energy dependence of directed flow slope for protons in 10-40% centrality Au+Au from the STAR experiment, compared with recent hybrid [94] and 3FD [95] model calculations. All the experimental data are from Ref. [46] except for one energy point, $\sqrt{s_{NN}}$ = 14.5 GeV [90], which should be considered a preliminary measurement.

3FD model [95] (see Fig. 14) is currently more than an order of magnitude larger than the experimental measurement being interpreted, and is larger still than the error on the measured data.

VI. SUMMARY AND OUTLOOK

In this review, we discuss heavy ion directed flow results for charged particles and for identified particle types, covering beam energies from the Brookhaven AGS to the CERN LHC. Charged particle directed flow measurements have been published as a function of transverse momentum, pseudorapidity, and collision centrality, while Cu+Cu and Au+Au have also been compared. The charged particle directed flow magnitude at the LHC is a factor of three smaller than that at top RHIC energy. The observations from RHIC suggest that the charged particle directed flow is independent of system size, but depends on the incident beam energy. Limiting fragmentation scaling is observed for v_1 at RHIC energies, but entropy-driven multiplicity scaling in terms of $dN_{\rm ch}/d\eta$ is not seen at RHIC. In mass-asymmetric collisions, specifically Cu+Au, recent directed flow measurements at $\sqrt{s_{NN}}$ = 200 GeV have opened a new window into quark and antiquark formation at the very earliest times of the collision evolution ($t \leq 0.25$ fm/c) and could clarify theoretical and experimental questions related to the Chiral Magnetic Effect and the Chiral Magnetic Wave.

Measurements of v_1 for identified species offer deeper insights into the development of hydrodynamic flow. Opposite v_1 for pions and protons at AGS/SPS and at lower RHIC energies suggests an important role for nuclear shadowing. Signals of anti-flow of neutral kaons in AGS/E895 together with kaon measurements in the RHIC Beam Energy Scan region point to kaon-nucleon potential effects. The single sign-change in proton v_1 slope and a double sign-change in net-proton v_1 slope, with a clear minimum around $\sqrt{s_{NN}} \sim$ 11.5 - 19.6 GeV shows a qualitative resemblance to a hydrodynamic model prediction called "softest point collapse of flow". This original prediction assumed a first-order phase transition, but a crossover from hadron gas to a deconfined phase can also cause a softening (a drop in pressure). None of the current state-of-the-art models can explain the main features of the STAR directed flow measurements, and different models with nominally similar equations of state diverge from each other very widely over the BES range.

Looking ahead to likely developments during the period 2017-2018 in the area of directed flow at $\sqrt{s_{NN}}$ of a few GeV and above, we can expect new BES Phase-I results for the ϕ meson, as well as final publication of current preliminary RHIC Beam Energy Scan Phase-I results, like those in Ref. [90]. We can also expect parallel theoretical work on related physics and interpretation of the newest data. The preliminary results

for new particle species like Λs and charged and neutral kaons, as well as BES v_1 for protons, Λs and pions in narrow bins of centrality (nine bins spanning 0-80% centrality) amount to very stringent constraints on the next round of theoretical interpretation in terms of the QCD phase diagram and equation of state.

More comprehensive measurements of the many phenomenological aspects of directed flow outlined in this review will be possible beginning in the year 2019, as a consequence of the much increased statistics of Phase-II of the RHIC Beam Energy Scan (to take data in 2019 and 2020), in conjunction with the anticipated upgrades to the performance of the STAR detector [101]. Thereafter, new facilities like FAIR [102] in Germany, NICA [103] in Russia, and J-PARC-HI [104, 105] in Japan, will begin coming online. These new dedicated facilities will further strengthen worldwide research on the QCD phase diagram at high baryon chemical potential.

Conflict of Interests

The authors declare that there is no conflict of interests regarding the publication of this paper.

Acknowledgments

This work was supported in part by the Office of Nuclear Physics within the US DOE Office of Science, under grant DE-FG02-89ER40531. We are grateful to the following colleagues for insightful advice and discussions: J. Auvinen, H. Caines, D. Cebra, V. Dexheimer, M. Lisa, W. Llope, G. Odyniec, Y. Pandit, H. Petersen, A. Poskanzer, H. G. Ritter, J. Steinheimer, H. Stöcker, A. H. Tang, S. Voloshin, G. Wang, N. Xu, and Z. Xu.

[1] I. Arsene *et al.* (BRAHMS Collaboration), Nucl. Phys. **A757**, 1 (2005).
[2] B. B. Back *et al.* (PHOBOS Collaboration), Nucl. Phys. **A757**, 28 (2005).
[3] J. Adams *et al.* (STAR Collaboration), Nucl. Phys. **A757**, 102 (2005).
[4] K. Adcox *et al.* (PHENIX Collaboration), Nucl. Phys. **A757**, 184 (2005).
[5] B. Muller and J. L. Nagle, Annu. Rev. Nucl. Part. Sci. **56**, 93 (2006).
[6] B. Jacak and P. Steinberg, Phys. Today **63N5**, 39 (2010).
[7] S. A. Bass *et al., Hot & Dense QCD Matter*, White Paper submitted to the 2012 Nuclear Science Advisory Committee; https://www.bnl.gov/npp/docs/Bass_RHI_WP_final.pdf
[8] W. Reisdorf and H. G. Ritter, Annu. Rev. Nucl. Part. Sci. **47**, 663 (1997).
[9] H. Sorge, Phys. Rev. Lett. **78**, 2309 (1997).
[10] N. Herrmann, J. P. Wessels and T. Wienold, Annu. Rev. Nucl. Part. Sci. **49**, 581 (1999).
[11] M. Gyulassy, K. A. Frankel and H. Stöcker, Phys. Lett. **110B**, 185 (1982).
[12] P. Danielewicz and M. Gyulassy, Phys. Lett. **129B**, 283 (1983).
[13] H. A. Gustafsson *et al.*, Phys. Rev. Lett. **52**, 1590 (1984).
[14] S. Voloshin and Y. Zhang, Z. Phys. C **70**, 665 (1996).
[15] A. M. Poskanzer and S. A. Voloshin, Phys. Rev. C **58**, 1671 (1998).
[16] A. Bilandzic, R. Snellings and S. Voloshin, Phys. Rev. C **83**, 044913 (2011).
[17] D. Teaney and L. Yan, Phys. Rev. C **83**, 064904 (2011).
[18] M. Luzum and J. Y. Ollitrault, Phys. Rev. Lett. **106**, 102301 (2011).
[19] Y. Nara, A. Ohnishi, and H. Stöcker, arXiv:1601.07692 [hep-ph].
[20] V. P. Konchakovski, W. Cassing, Yu. B. Ivanov and V. D. Toneev, Phys. Rev. C **90**, 014903 (2014).
[21] U. W. Heinz, in *Relativistic Heavy Ion Physics*, Landolt-Boernstein New Series, Vol. I/23, edited by R. Stock (Springer Verlag, New York, 2010).
[22] H. Stöcker, Nucl. Phys. **A750**, 121 (2005).
[23] S. A. Bass et al., Prog. Part. Nucl. Phys. **41**, 255 (1998).
[24] M. Bleicher, E. Zabrodin, C. Spieles, S. A. Bass, C. Ernst, S. Soff, L. Bravina, M. Belkacem, H. Weber, H. Stöcker and W. Greiner, J. Phys. G **25**, 1859 (1999).
[25] S. Z. Belenkij and L. D. Landau, Nuovo Cimento Suppl. **3**, 15 (1956).
[26] G. F. Chapline, M. H. Johnson, E. Teller and M. S. Weiss, Phys. Rev. D **8**, 4302 (1973).
[27] W. Scheid, H. Müller and W. Greiner, Phys. Rev. Lett. **32**, 741 (1974).
[28] J. Hofmann, H. Stöcker, U. Heinz, W. Scheid and W. Greiner, Phys. Rev. Lett. **36**, 88 (1976).
[29] H. Stöcker, J. A. Maruhn and W. Greiner, Phys. Rev. Lett. **44**, 725 (1980).
[30] J. Barrette *et al.* (E877 Collaboration), Nucl. Phys. **A590**, 259c (1995).
[31] J. Barrette *et al.* (E877 Collaboration), Phys. Rev. C **56**, 3254 (1997).
[32] J. Barrette *et al.* (E877 Collaboration), Phys. Rev. C **59**, 884 (1999).
[33] J. Barrette *et al.* (E877 Collaboration), Phys. Lett. **B485**, 319 (2000).

[34] H. Liu *et al.* (E895 Collaboration), Phys. Rev. Lett. **84**, 5488 (2000).
[35] P. Chung *et al.* (E895 Collaboration), Phys. Rev. Lett. **85**, 940 (2000).
[36] P. Chung *et al.* (E895 Collaboration), Phys. Rev. Lett. **86**, 2533 (2001).
[37] C. Pinkenburg *et al.* (E895 Collaboration), Proc. of Quark Matter 2001, Stony Brook, New York, Nucl. Phys. **A698**, 495c (2002).
[38] C. Alt *et al.* (NA49 Collaboration), Phys. Rev. Lett. **80**, 4136 (1998).
[39] C. Alt *et al.* (NA49 Collaboration), Phys. Rev. C **68**, 034903 (2003).
[40] J. Adams *et al.* (STAR Collaboration), Phys. Rev. C **72**, 014904 (2005).
[41] B. B. Back *et al.* (PHOBOS Collaboration), Phys. Rev. Lett. **97**, 012301 (2006).
[42] J. Adams *et al.* (STAR Collaboration), Phys. Rev. C **73**, 034903 (2006).
[43] B. I. Abelev *et al.* (STAR Collaboration), Phys. Rev. Lett. **101**, 252301 (2008).
[44] G. Agakishiev *et al.* (STAR Collaboration), Phys. Rev. C **85**, 014901 (2012).
[45] L. Adamczyk *et al.* (STAR Collaboration), Phys. Rev. Lett. **108**, 202301 (2012).
[46] L. Adamczyk *et al.* (STAR Collaboration), Phys. Rev. Lett. **112**, 162301 (2014).
[47] L. P. Csernai and D. Rohrich, Phys. Lett. B **458**, 454 (1999).
[48] J. Brachmann *et al.*, Phys. Rev. C **61**, 024909 (2000).
[49] R. J. M. Snellings, H. Sorge, S. A. Voloshin, F. Q. Wang and N. Xu, Phys. Rev. Lett. **84**, 2803 (2000).
[50] Y. Guo, F. Liu, and A. H. Tang, Phys. Rev. C **86**, 044901 (2012).
[51] P. Bozek and I. Wyskiel, Phys. Rev. C **81**, 2803 (2000).
[52] STAR ZDC-SMD proposal, STAR Note SN-0448 (2003).
[53] G. Wang, PhD thesis, Kent State University, 2005; https://drupal.star.bnl.gov/STAR/theses.
[54] The STAR ZDC-SMD has the same structure as the STAR EEMC SMD: C. E. Allgower *et al.*, Nucl. Instr. Meth. A **499**, 740 (2003).
[55] B. Abelev *et al.* (ALICE Collaboration), Phys. Rev. Lett. **111**, 232302 (2013).
[56] U. Heinz and P. Kolb, J. Phys. G **30**, S1229 (2004).
[57] J. Adams *et al.* (STAR Collaboration), Phys. Lett. B **655**, 104 (2007).
[58] J. Bleibel, G. Burau, and C. Fuchs, Phys. Lett. B **659**, 520 (2008).
[59] L. P. Csernai, V. K. Magas, H. Stöcker, and D. D. Strottman, Phys. Rev. C **84**, 024914 (2011).
[60] Z.-W. Lin and C. M. Ko, Phys. Rev. C **65**, 034904 (2002).
[61] Z.-W. Lin, C. M. Ko, B.-A. Li, B. Zhang and S. Pal, Phys. Rev. C **72**, 064901 (2005).
[62] L.-W. Chen, V. Greco, C. M. Ko and P. F. Kolb, Phys. Lett. **B605**, 95 (2005).
[63] R. P. Feynman, Phys. Rev. Lett. **23**, 1415 (1969).
[64] J. Benecke, T. T. Chou, C.-N. Yang and E. Yen, Phys. Rev. **188**, 2159 (1969).
[65] H. Caines, Eur. Phys. J. **C49**, 297 (2007); arXiv:nucl-ex/0609004.
[66] H. Caines, private communication, 2016.
[67] M. Lisa, arXiv:nucl-ex/0512008.
[68] B. Alver *et al.* (PHOBOS Collaboration), Phys. Rev. Lett. **98**, 242302 (2007).
[69] A. Adare *et al.* (PHENIX Collaboration), submitted to Phys. Rev. C; arXiv:1509.07784v1.
[70] L. Adamczyk *et al.* (STAR Collaboration), submitted for publication; arXiv:1608.04100.
[71] W. Cassing, Eur. Phys. J.: Spec. Top. **168**, 3 (2009).
[72] V. Voronyuk, V. D. Toneev, S. A. Sergei and W. Cassing, Phys. Rev. C **90**, 064903 (2014).
[73] https://www.desy.de/h1zeus/combined_results/herapdftable/
[74] D. Kharzeev, R. D. Pisarski and M. H. G. Tytgat, Phys. Rev. Lett. **81**, 512 (1998).
[75] D. Kharzeev and R. D. Pisarski, Phys. Rev. D **61**, 111901 (2000).
[76] D. E. Kharzeev and H. Yee, Phys. Rev. D **83**, 085007 (2011).
[77] Y. Burnier, D. E. Kharzeev, J. Liao, and H.-U. Yee, Phys. Rev. Lett. **107**, 052303 (2011).
[78] S. A. Voloshin, Phys. Rev. C 55, R1630 (1997).
[79] P. Kolb and U. Heinz, nucl-th/0305084.
[80] P. Huovinen and P.V. Ruuskanen, Annu. Rev. Nucl. Part. Sci. **56**, 163 (2006).
[81] N. Borghini, P. M. Dinh, and J.-Y. Ollitrault, Phys. Rev. C **66**, 014905 (2002).
[82] P. Danielewicz and G. Odyniec, Phys. Lett. **157B**, 146 (1985).
[83] M. D. Partlan *et al.* (EOS Collaboration), Phys. Rev. Lett. **75**, 2100 (1995).
[84] M. Isse, A. Ohnishi, N. Otuka, P. K. Sahu and Y. Nara, Phys. Rev. C **72**, 064908 (2005).
[85] B. I. Abelev *et al.* (STAR collaboration), STAR Note SN0493 (2009).
[86] M. M. Aggarwal *et al.* (STAR collaboration), arXiv:1007.2613.
[87] F. Karsch *et al.*, Nucl. Phys. B Proc. Suppl. **129**, 614 (2004).
[88] Y. Aoki, G. Endrodi, Z. Fodor, S. D. Katz and K. K. Szabo, Nature **443**, 675 (2006).
[89] M. Cheng *et al.*, Phys. Rev. D **79**, 074505 (2009).
[90] P. Shanmuganathan for the STAR Collaboration, Proc. of Quark Matter 2015, Kobe, Japan, Nucl. Phys. **A** (in press); arXiv:1512.09009v1.
[91] W. Cassing, V. P. Konchakovski, A. Palmese, V. D. Toneev and E. L. Bratkovskaya, Proc. 3rd Int. Conf. on New Frontiers in Physics, Kolymbari, Crete, 2014, EPJ Web Conf. **95**, 01004 (2015); arXiv:1408.4313 [nucl-th].
[92] P. Shukla, A. K. Mohanty, Phys. Rev. C **64**, 054910 (2001).

[93] A. Bessa, E. S. Fraga, B. W. Mintz, Phys. Rev. D **79**, 034012 (2009).
[94] J. Steinheimer, J. Auvinen, H. Petersen, M. Bleicher and H. Stöcker, Phys. Rev. C **89**, 054913 (2014).
[95] Yu. B. Ivanov and A. A. Soldatov, Phys. Rev. C **91**, 024915 (2015).
[96] H. Petersen, J. Steinheimer, G. Burau, M. Bleicher and H. Stöcker, Phys. Rev. C **78**, 044901 (2008).
[97] Yu. B. Ivanov, V. N. Russkikh, and V. D. Toneev, Phys. Rev. C **73**, 044904 (2006).
[98] Y. Nara, N. Otuka, A. Ohnishi, K. Niita and S. Chiba, Phys. Rev. C **61**, 024901 (2000).
[99] D. E. Kahana, D. Keane, Y. Pang, T. Schlagel and S. Wang, Phys. Rev. Lett. **74**, 4404 (1995).
[100] D. E. Kahana, Y. Pang and E. V. Shuryak, Phys. Rev. C **56**, 481 (1997).
[101] STAR collaboration, BES Phase-II Whitepaper, STAR Note SN0598 (2014).
[102] http://www.fair-center.eu
[103] http://nica.jinr.ru/tech.html
[104] H. Sako *et al.*, Nucl. Phys. **A 931**, 1158 (2014).
[105] H. Sako *et al.*, White Paper for J-PARC Heavy-Ion Program, April 2016,
http://silver.j-parc.jp/sako/white-paper-v1.17.pdf